

Weakly invasive metrology: quantum advantage and physical implementations

M. Perarnau-Llobet,^{1,2,3} D. Malz,^{1,2} and J. I. Cirac^{1,2}

¹*Max-Planck-Institut für Quantenoptik, D-85748 Garching, Germany.*

²*Munich Center for Quantum Science and Technology (MCQST), Schellingstrasse 4, D-80799 München*

³*Département de Physique Appliquée, Université de Genève, Genève, Switzerland*

(Dated: November 8, 2021)

We consider the estimation of a Hamiltonian parameter of a set of highly photosensitive samples, which are damaged after a few photons N_{abs} are absorbed. The samples are modelled as a two mode photonic system, where photons simultaneously acquire information on the unknown parameter and are absorbed at a fixed rate. We show that arbitrarily intense coherent states can obtain information at a rate that scales at most linearly with N_{abs} , whereas quantum states with finite intensity can overcome this bound. The quantum advantage scales like N/N_{abs} (where N is the number of photons in the quantum state), so that few-photon entangled states can already surpass the classical bound when N_{abs} is small. We discuss an implementation in cavity QED, where Fock states are both prepared and measured by coupling atomic ensembles to the cavities.

INTRODUCTION

One exciting prospect of quantum technologies are more precise photonic measurements through the use of quantum correlations [1–5]. Given a fixed (average) photon number N , a variety of quantum states surpasses the shot-noise limit imposed by coherent states, notably squeezed, NOON or twin Fock states [6–8]. One of the motivations to limit N is that some photosensitive materials, such as biological samples [9–14], may be damaged when they absorb too many photons. However, in this case it may be more meaningful to constrain the number of photons absorbed by the sample N_{abs} , instead of N [15]. While in interferometric measurements this constraint is equivalent to fixing the total number of photons, we will show here it leads to qualitatively new results in frequency measurements in which photons are allowed to interact continuously with the sample.

In order to compare different approaches in metrology, one has to clearly define the constraints and resources involved. Here we consider the measurement of a Hamiltonian parameter (with units of frequency) of a set of identical samples. We set as constraints the total time T of the experiment and N_{abs} , the number of photons that the sample can tolerate before being damaged or destroyed, and leave the photon number N unconstrained –in contrast to previous works on frequency measurements in atomic ensembles [16–21]. The samples are processed sequentially, and the same test is applied to each of them. Under those constraints, we prove that quantum metrological protocols involving a small amount $N \approx 5 - 10$ of photons (prepared in NOON or twin-Fock states) and a finite amount of samples, can overcome classical strategies using coherent states of (potentially) arbitrary intensity and an arbitrarily large number of samples. We also derive general upper and lower bounds on the quantum advantage as a function of N_{abs} , and show that such enhancements can be realized in state-of-the-art technologies using a cavity or circuit QED set-up [22, 23].

FRAMEWORK AND PHYSICAL SETUP

We model the “delicate sample” as a two-mode photonic system, $H = H_0 + gH_{\text{int}}$ with $H_0 = \omega(a^\dagger a + b^\dagger b)$ and $H_{\text{int}} = (a^\dagger b + ab^\dagger)/2$. We wish to estimate the interaction strength g between modes (g has units of frequency and we set $\hbar = 1$). The inference process is mediated by photons, which can also be absorbed by the sample leading to its degradation. The latter process is modelled as a Markovian dissipative process, so that the whole time evolution of the quantum photonic state ρ reads:

$$\dot{\rho} = -i[H_0 + gH_{\text{int}}, \rho] + \gamma(\mathcal{D}_a(\rho) + \mathcal{D}_b(\rho)) \quad (1)$$

with $\mathcal{D}_x(A) = xAx^\dagger - \frac{1}{2}\{x^\dagger x, A\}$. With time, information on g is encoded in ρ , but also photons are lost (absorbed). These two dynamical processes decouple –i.e., the unitary and dissipative parts of the dynamics commute–, so that the evolution can be described as two independent channels: $\rho(t) = \mathcal{C}_{g,t}^{\text{uni}} \circ \mathcal{C}_{\gamma,t}^{\text{diss}}[\rho_0]$, with $\mathcal{C}_{\gamma,t}^{\text{diss}}[\rho] = e^{-\gamma t(\mathcal{D}_a + \mathcal{D}_b)}[\rho]$ and $\mathcal{C}_{g,t}^{\text{uni}}[\rho] = e^{-i(H_0 + gH_{\text{int}})t} \rho e^{i(H_0 + gH_{\text{int}})t}$.

If the initial state ρ_0 contains N photons, the (average) number of absorbed photons is given by

$$N_{\text{abs}}(t) = \text{Tr}[\rho(t)\hat{N}] = N(1 - e^{-\gamma t}), \quad (2)$$

where $\hat{N} = a^\dagger a + b^\dagger b$ counts the total number of photons. We shall assume that the delicate sample is destroyed when $N_{\text{abs}}(t) = N_{\text{abs}}$, which sets a maximum available time for information acquisition. This constrains the possible estimation schemes and, to some extent, N_{abs} can be seen as a resource: a larger N_{abs} enables us to obtain more information (and/or in a faster manner) from a single sample.

In order to estimate g , we consider the following metrological scenario: We have at our disposal a large number of delicate samples that we can measure sequentially for a total time T . The same estimation scheme, or test, is applied to each sample. In each test, a photonic state ρ_0 is prepared, it evolves for some time t according to (1) reaching ρ_g , and is measured by a (generalized) quantum observable Π , which yields the outcome s_j with probability p_j . The whole

experiment consists of ν tests, with each test taking a time $t = T/\nu$, which must satisfy $N_{\text{abs}}(t) \leq N_{\text{abs}}$. Note that no assumptions are made neither on the number of photons in the initial state ρ_0 nor on the number of tests ν ; only N_{abs} and T are constrained. When $\nu \gg 1$ (the regime of interest in this paper), the uncertainty $\Delta^2 g$ of an unbiased estimator of g satisfies [24–26]:

$$\Delta^2 g \geq \frac{1}{\nu \mathcal{F}_C} \geq \frac{1}{\nu \mathcal{F}_Q}. \quad (3)$$

Here, $\mathcal{F}_C = \sum_j p_j^{-1} (\partial p_j / \partial g)^2$ is the Classical Fisher Information (CFI) and \mathcal{F}_Q is the quantum Fisher Information (QFI), which will be defined later for each case of interest, and characterizes the potential of ρ_g for estimating g with an optimal measurement [26]. Our goal is to minimize (3) for both classical (i.e. coherent) and quantum (e.g. Fock, or NOON) states, and to find the corresponding optimal strategies.

It is worth pointing out that, defining $a_{\pm} \equiv (a \pm b^{\dagger})/\sqrt{2}$, we can rewrite H as $H = (\omega + g)a_{+}^{\dagger}a_{+} + (\omega - g)a_{-}^{\dagger}a_{-}$, so an alternative interpretation of this framework is that we are estimating the frequency difference between two modes. In terms of the original modes a and b , both pictures are physically equivalent if a balanced beamsplitter is applied to the input (and output) light. With this transformation, it is also clear that the problem at hand can be formally mapped to standard Mach-Zehnder interferometry with $\varphi = gt$, where photon absorption corresponds to a symmetric (time-dependent) photon loss. This map naturally enables us to use techniques and results developed in this context [1–3].

OPTIMAL CLASSICAL STRATEGY

Let us first analyze the optimal strategy using coherent states. We consider as an input state $\rho_0 = |g_0\rangle\langle g_0|$ with $|g_0\rangle = |\cos(\theta)\sqrt{N}, \sin(\theta)\sqrt{N}\rangle$. The dissipative channel acts upon the initial state as $|\phi\rangle = \mathcal{C}_{\gamma,t}^{\text{diss}}|g_0\rangle = |\cos(\theta)\sqrt{e^{-\gamma t}N}, \sin(\theta)\sqrt{e^{-\gamma t}N}\rangle$. Since the state remains pure, we can quantify the QFI of $\rho_g = \mathcal{C}_{g,t}^{\text{uni}}[|\phi\rangle\langle\phi|]$ as $\mathcal{F}_Q = 4t^2(\langle\phi|H_{\text{int}}^2|\phi\rangle - (\langle\phi|H_{\text{int}}|\phi\rangle)^2)$ [26], obtaining: $\mathcal{F}_Q^{\text{coh}} = t^2Ne^{-\gamma t}$ (this is the shot-noise-limit). On the other hand, the number of loss photons is $N_{\text{abs}} = N(1 - e^{-\gamma t})$; using $t = T/\nu$, yields:

$$\nu \mathcal{F}_Q^{\text{coh}} = \frac{T^2}{\nu} N_{\text{abs}} \frac{e^{-\gamma T/\nu}}{1 - e^{-\gamma T/\nu}}. \quad (4)$$

Eq. (4) increases monotonically with ν , so its maximum $(\Delta g)^{-2}_{\text{coh}} \equiv \max_{\nu}(\nu \mathcal{F}_Q^{\text{coh}})$ is obtained in the limit $\nu \rightarrow \infty$:

$$(\Delta g)^{-2}_{\text{coh}} = \frac{T}{\gamma} N_{\text{abs}}. \quad (5)$$

Strictly speaking, this bound can be saturated by testing $\nu \rightarrow \infty$ samples, each for an infinitesimally small time $t \rightarrow 0$ using $N \rightarrow \infty$ photons, in such a way that

both $N_{\text{abs}} = \gamma t N$ and $T = \nu t$ remain constant. We call this theoretical limit ($N, \nu \rightarrow \infty$ and $t \rightarrow 0$, with both $N_{\text{abs}} = \gamma t N$ and $T = \nu t$ fixed) the *Poisson limit*, or *Poisson regime*, which will play a relevant role in this work. The importance of the classical bound (5) is that it remains finite – being limited by both T and N_{abs} – despite using an infinite amount of photons (at each test) and an infinite number of tests. We also note that optimality of fast measurements has also been found in frequency measurements of atomic ensembles [16–21].

QUANTUM STRATEGIES: TWIN FOCK STATES

We now move to quantum resources. We focus on the paradigmatic case of twin-Fock states [7, 27]. As in the previous case, we wish to maximize $(\Delta g)^{-2}_{\text{TFS}} \equiv \max_{\nu}(\nu \mathcal{F}_Q)$ given some T and N_{abs} .

In order to compute the QFI, we note that given $\rho_g = \sum_s q_s |\phi_s(t)\rangle\langle\phi_s(t)|$, with $|\phi_s(t)\rangle = e^{-itgH_{\text{int}}}|\phi_s\rangle$ and $\langle\phi_s|\phi_l\rangle = \delta_{sl}$; the QFI reads $\mathcal{F}_Q = 4t^2 \left[\sum_i q_i (\Delta H_i)^2 - \sum_{i \neq j} 2q_i q_j |H_{ij}|^2 (q_i + q_j)^{-1} \right]$, with $(\Delta H_i)^2 = \langle\phi_i|H_{\text{int}}^2|\phi_i\rangle - (\langle\phi_i|H_{\text{int}}|\phi_i\rangle)^2$ and $|H_{ij}|^2 = |\langle\phi_i|H_{\text{int}}|\phi_j\rangle|^2$ [26, 28]. In our case, the initial state is $\rho_0 = |\phi_0\rangle\langle\phi_0|$ with $|\phi_0\rangle = |n, n\rangle$ and $N = 2n$, and evolves in time as: $\rho_g = \sum_{k,j} p_k p_j |\phi_{k,j}(t)\rangle\langle\phi_{k,j}(t)|$ with $|\phi_{k,j}\rangle = e^{-itgH_{\text{int}}} |n-k, n-j\rangle$, $p_k = \binom{n}{k} \mu^k (1-\mu)^{n-k}$ and $\mu = 1 - e^{-\gamma t}$. We hence obtain,

$$\mathcal{F}_Q = 4t^2 \sum_{ij}^n p_i p_j (n-i)(n-j+1) \left(\frac{1}{2} - \frac{1}{1 + \frac{(n-j+1)(i+1)}{j(n-i)}} \right). \quad (6)$$

In the Poisson limit ($t \rightarrow 0$ and $n \rightarrow \infty$ with $2n\gamma t = N_{\text{abs}}$),

$$\mathcal{F}_Q = \frac{N_{\text{abs}}^2}{\gamma^2} \sum_{ij}^{\infty} p_i p_j \left(\frac{1}{2} - \frac{j}{i+1+j} \right) \equiv \frac{\mathcal{G}(N_{\text{abs}})}{\gamma^2}, \quad (7)$$

with

$$p_k = \frac{(N_{\text{abs}}/2)^k e^{-N_{\text{abs}}/2}}{k!}. \quad (8)$$

For $N_{\text{abs}} \gg 1$, the Poisson distribution (8) is strongly peaked around $k = N_{\text{abs}}/2$, such that the sum in (7) is dominated by $i = j = N_{\text{abs}}/2$. In this regime, $\mathcal{F}(N_{\text{abs}}) \approx N_{\text{abs}}/2$. In contrast, as $N_{\text{abs}} \rightarrow 0$, $\mathcal{F}(N_{\text{abs}}) \approx N_{\text{abs}}^2/2$. Eq. (7) is finite for $N_{\text{abs}} > 0$, which means that a finite amount of information is obtained as $t \rightarrow 0$. This implies that $(\Delta g)^2_{\text{TFS}} = (\nu \mathcal{F}_Q)^{-1} \rightarrow 0$ in the Poisson regime ($\nu \rightarrow \infty$, $tv = T$, $N\gamma t = N_{\text{abs}}$). That is, g can in principle be estimated with arbitrary precision using TFS given any $T, N_{\text{abs}} > 0$.

This advantage assumes the possibility of creating Fock states of arbitrary large photon number,

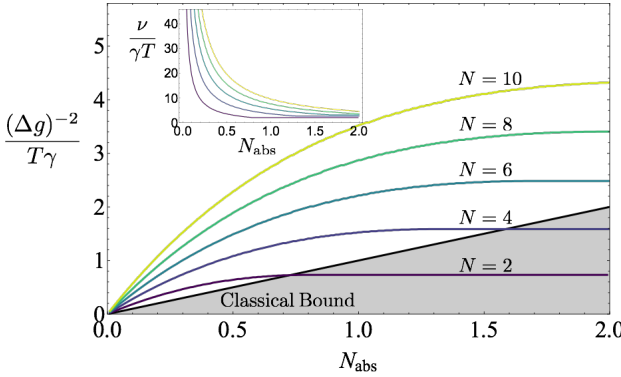


Figure 1. $(\Delta g)^{-2} \equiv \nu \mathcal{F}_Q$ per unit of time as a function of N_{abs} for twin Fock states (TFS) of low N , together with the classical bound (5) for coherent states corresponding to the limit $N \rightarrow \infty$, $\nu \rightarrow \infty$. The numerical results for TFS are obtained by computing $\max_{\nu} (\nu \mathcal{F}_Q)$ given the constraints $t\nu = T$ and $N_{\text{abs}}(t) \leq N_{\text{abs}}$ with $N_{\text{abs}}(t)$ in (2). The optimal ν for TFS, which satisfies $\nu/T\gamma \approx N/N_{\text{abs}}$, is shown in the inset. Overall, we find good qualitative agreement between the numerical results obtained for low N and the analytical considerations where $N \gg 1$ is used. These results confirm the possibility of noticeable quantum advantages using low-photon entangled states over coherent states of arbitrary intensity. For performing the plot, we take $T = 10$ and $\gamma = 1$, but essentially the same results are obtained for larger T . We also note that the bound (3) becomes more accurate as T , and hence ν , increases.

which should be prepared and measured arbitrarily fast; this is arguably impossible experimentally. It is hence necessary to understand to which extent the classical bound (5) can be surpassed with Fock states of a maximal finite number n , with $N = 2n$. If $N \gg 1$ (and $N \gg N_{\text{abs}}$), using (2) we can replace $\nu/\gamma^2 = T/(t\gamma^2) \approx TN/(t\gamma N_{\text{abs}})$ in (7) to obtain $(\Delta g)_{\text{TFS}}^{-2} \approx TN\mathcal{G}(N_{\text{abs}})/\gamma N_{\text{abs}}$, and hence

$$(\Delta g)_{\text{TFS}}^{-2} \approx \begin{cases} TNN_{\text{abs}}/2\gamma & \text{for } N_{\text{abs}} \lesssim 1 \\ TN/2\gamma & \text{for } N_{\text{abs}} \gtrsim 1 \end{cases}$$

Crucially, the quantum advantage $(\Delta g)_{\text{coh}}^2 / (\Delta g)_{\text{TFS}}^2$ is proportional to N , so that few-photon entangled states already provide an advantage with respect to coherent states of arbitrary intensity in this metrological task. This is the main result of this work, which is illustrated numerically in Fig. 1 in the experimentally relevant regime of low N and N_{abs} . The results are obtained by the exact expression (6) and by testing a finite number of samples $\nu = \mathcal{O}(NT\gamma/N_{\text{abs}})$ for a finite time $t = T/\nu$ (see details in the inset of Fig. 1). As an example, given a delicate sample that may absorb at most one photon ($N_{\text{abs}} = 1$), more information per unit time can be obtained by performing tests at a rate of 5 samples per γ^{-1} (the absorption timescale) using TFS of 4 photons than by any possible strategy using coherent states of potentially arbitrary intensity.

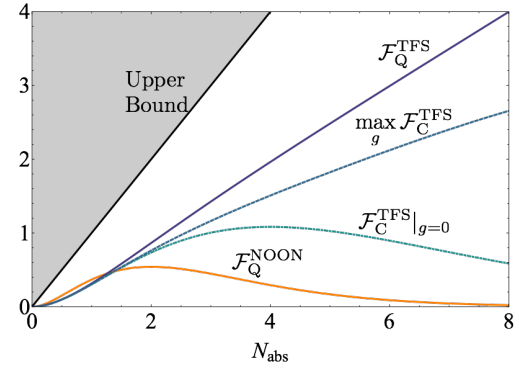


Figure 2. The QFI as a function of N_{abs} for TFS (purple) and NOON (orange) states in the Poisson limit ($t \rightarrow 0$, $N \rightarrow \infty$ with $N_{\text{abs}} = \gamma t N$ fixed), together with the upper bound (10). In dashed lines, we show the classical Fisher Information \mathcal{F}_C for TFS with $g = 0$ (turquoise) and maximized over $g \in (0, 2\pi)$ (blue). Details on the calculation of \mathcal{F}_C for TFS are provided in the Appendix, see also Refs. [29, 30]. Only states with Heisenberg scaling can yield non-zero information in this plot. Parameters: $\gamma = 1$.

FUNDAMENTAL LOWER AND UPPER BOUNDS

Before considering explicit implementations where such quantum advantages can be witnessed using TFS, we derive some general considerations on quantum states in the Poisson regime. Assume that a pure N -photon state $|\phi\rangle$ has Heisenberg scaling, i.e., $\mathcal{F}_Q[|\phi\rangle] = c_\phi N^2 t^2$ with $0 < c_\phi \leq 1$. Then, in the presence of photon loss, the QFI of the corresponding mixed state ρ_ϕ in the Poisson regime ($t \rightarrow 0$ with $Nt = N_{\text{abs}}/\gamma$ constant) will be lower bounded by:

$$\mathcal{F}_Q[\rho_\phi] \geq \frac{c_\phi}{\gamma^2} N_{\text{abs}}^2 e^{-N_{\text{abs}}/\gamma}, \quad (9)$$

which is obtained by setting $k = 0$ in (8) and noting that the QFI is additive under subspaces with different photon number. For example, NOON states saturate this lower bound with $c_\phi = 1$. On the other hand, these considerations also show that

Only quantum states with Heisenberg scaling can obtain a finite amount of information per absorbed photon in zero time.

This theoretical observation, which requires using an infinite number of photons, turns into practical quantum advantages with few-photon entangled states as shown in Fig. 1.

We can also obtain an upper bound using the results of Refs [31–34], where the bound $\mathcal{F}_Q \leq N(1 - \mu)/\mu$ is obtained for an optical interferometer set-up with symmetric photon loss in both arms, as quantified by μ (the probability of photon loss in each arm of the interferometer). For the problem at hand, this translates as $\mu = 1 - e^{-\gamma t}$ and $N_{\text{abs}} = \mu N$. Taking the Poisson limit ($t \rightarrow 0$ and N_{abs} constant) yields

$$\mathcal{F}_Q[\rho_\phi] \leq \frac{N_{\text{abs}}}{\gamma^2}. \quad (10)$$

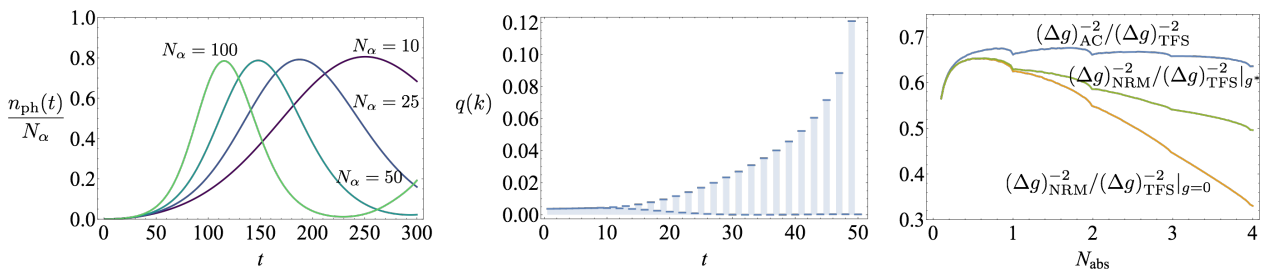


Figure 3. (a) Evolution of the average photon number $n_{\text{ph}}(t)$ in the cavity through the interaction (11). The initial state has N_α excited atoms and cavity in the ground state. The photon number is maximized at a time t^* where $n_{\text{ph}}(t^*)/N_\alpha \approx 0.8$. Parameters: $J = 1$, $\omega_0 = 1$. (b) Probability distribution of the photon number at t^* for $N_\alpha = 50$. Parameters: $J = 1$, $\omega_0 = 1$. (c) Measurement uncertainty for (i) the atom-cavity (AC) implementation with an optimal measurement $((\Delta g)_{\text{AC}}^{-2}$, in blue), (ii) the AC implementation with a NRM at an optimal $g = g^*$ $((\Delta g)_{\text{NRM}}^{-2}|_{g^*}$), and (iii) the AC implementation with a NRM at $g = 0$ $((\Delta g)_{\text{NRM}}^{-2}|_{g=0}$); the three of them compared to $(\Delta g)_{\text{TFS}}^{-2}$. Details of the calculation are provided in the SM.

Note that this upper bound cannot be saturated for $N_{\text{abs}} \ll 1$, which follows by expanding $\mathcal{F}_Q[\rho_\phi]$ around $N_{\text{abs}} \rightarrow 0$: $\mathcal{Q}_{\rho_\phi} = c_\phi N_{\text{abs}}^2/\gamma^2 + \mathcal{O}(N_{\text{abs}}^3)$ with $c_\phi \leq 1$. On the other hand, TFS obtain $1/2$ of the optimal upper bound for $N_{\text{abs}} \gtrsim 1$, which already provides a good approximation of optimal states. An overview of the different results obtained in the Poisson limit is shown in Fig. 2. It remains an interesting open question to investigate photonic states which can perform better than TFS in the Poisson regime, thus complementing the results of Refs. [31, 35–39] obtained for $N_{\text{abs}} \propto N$.

IMPLEMENTATION IN CAVITY QED

Perhaps the greatest challenge in observing quantum-enhanced metrology is producing and measuring quantum states of light, such as TFS, GHZ and NOON states. Here, we therefore outline a protocol based on cavity QED [22] or circuit QED [23] capable of generating and observing Fock states of light in cavities, inspired by recent progress on metrology and number-resolved measurements in waveguide QED [40–43]. The key idea is to engineer an interaction of the cavity with a set of resonant qubits/atoms, such that in addition to Eq. (1), the two cavities are each coupled to a collection of atoms via

$$H_{\text{Dicke}} = \sum_{\alpha=a,b} \sum_i^{N_\alpha} [\omega_0 \sigma_{i,\alpha}^z + J(t) (\sigma_{i,\alpha}^- \alpha^\dagger + \text{H.c.})]. \quad (11)$$

Let us suppose that $J(t)$ can be turned on and off at will, and that it is possible to measure the collective spin of the atoms $S_\alpha^z = \sum_i \sigma_{\alpha,i}^z$.

Starting from the ground state, a photonic Fock state in each cavity is produced following the following three steps. (i) All atoms are excited. (ii) The cavity-atom interaction is turned on, $J(t) = J$, for a time $t_{\text{opt}} \approx \log(4N_\alpha)/(2J\sqrt{N_\alpha})$. As we show in the SM and illustrate in Fig. 3a, this is the optimal waiting time for maximizing the photon number n_{ph} , leading to $n_{\text{ph}}/N_\alpha \approx 0.8$. (iii) The cavity-atom interaction is

turned off and S_α^z is measured. Conditional on the measurement outcome k_α , the cavity is projected in a Fock state with $N_\alpha - k_\alpha$ photons, with a probability distribution shown in Fig. 3b. This can be done in parallel for both cavities.

After this preparation stage, we let the photonic system evolve for some time t , which is the time relevant for our discussion in the rest of the article. In the mean time, the remaining k_α atoms need to be reset to the ground state in order to prepare them for the final measurement.

To measure the final photon distribution in the cavity, we again turn on the atom-cavity coupling $J(t)$, which allows the atoms to reabsorb photons from the cavity. After a time t_{opt} most of the photons are reabsorbed and we measure again the number of excited atoms and place them back into the ground state. Since this process likely fails to capture all photons, it has to be repeated until no photons are left in the cavities. Adding up the total number of excitations observed in the measurements yields the measurement result, thus implementing a number-resolved-measurement (NRM) in each cavity.

In ideal conditions, the discussed preparation scheme does not produce TFS, but rather Fock states distributed according Fig. 3b. This leads to a reduction in optimal measurement precision (i.e. Quantum Fisher Information \mathcal{F}_Q) of around a 30%, as illustrated in Fig. 3c and discussed in detail in the Appendix. In addition, the NRM in each cavity is in general not optimal for metrology, i.e., the corresponding CFI does not saturate \mathcal{F}_Q (see Fig. 2, Fig. 3c and the Appendix). Taking both effects into account, we find that the reported quantum advantages in Fig. 1 appear feasible in this implementation for small N_{abs} , while requiring the number of atomic excitations to be approximately twice as large as N (details in Fig. 3c and in the Appendix). Experimental requirements needed for the successful implementation of this proposal are discussed in the SM, where we argue that both cavity QED [44–46] and circuit QED [47–49] appear as promising platforms.

CONCLUSIONS

While quantum advantages in photonic metrology are well established when the (average) photon number is fixed [3–5], in specific situations, other constraints might be more meaningful. For example, when non-linear effects or quantum backaction limit the light intensity, a more sophisticated analysis has to take these effects into account [50]. Here, we study a complimentary situation, where photosensitive samples imply that the number of absorbed photons is limited [9–13, 15]. While in interferometric measurements this coincides with the traditional constraint on N , we have shown that it leads to qualitatively new results in frequency measurements. In this case, finite quantum resources for metrology (finite photon number, finite number of samples, finite time) become more powerful than infinite classical resources (unbounded photon number, unlimited number of samples, finite time). We have characterized these advantages for a model of two coupled oscillators, which can be realized in a cavity QED set-up, but our results suggest similar advantages in frequency measurements of delicate samples where photon absorption can be modelled as a Markovian process.

Acknowledgements. We thank J. Kołodyński and M. W. Mitchell for insightful discussions. M. P.-L. acknowledges funding from Swiss National Science Foundation (Ambizione PZ00P2-186067). D.M. and J.I.C. acknowledge funding from ERC Advanced Grant QENOCOBA under the EU Horizon 2020 program (Grant Agreement No. 742102).

[1] V. Giovannetti, S. Lloyd, and L. Maccone, *Nature Photonics* **5**, 222 (2011).

[2] G. Tóth and I. Apellaniz, *Journal of Physics A: Mathematical and Theoretical* **47**, 424006 (2014).

[3] R. Demkowicz-Dobrzański, M. Jarzyna, and J. Kołodyński, in *Progress in Optics* (Elsevier, 2015) pp. 345–435.

[4] J. P. Dowling and K. P. Seshadreesan, *Journal of Lightwave Technology* **33**, 2359 (2015).

[5] E. Polino, M. Valeri, N. Spagnolo, and F. Sciarrino, arXiv preprint arXiv:2003.05821 (2020).

[6] C. M. Caves, *Phys. Rev. D* **23**, 1693 (1981).

[7] M. J. Holland and K. Burnett, *Phys. Rev. Lett.* **71**, 1355 (1993).

[8] J. J. Bollinger, W. M. Itano, D. J. Wineland, and D. J. Heinzen, *Phys. Rev. A* **54**, R4649 (1996).

[9] T. Ono, R. Okamoto, and S. Takeuchi, *Nature Communications* **4** (2013), 10.1038/ncomms3426.

[10] M. A. Taylor, J. Janousek, V. Daria, J. Knittel, B. Hage, H.-A. Bachor, and W. P. Bowen, *Nature Photonics* **7**, 229 (2013).

[11] M. A. Taylor, J. Janousek, V. Daria, J. Knittel, B. Hage, H.-A. Bachor, and W. P. Bowen, *Phys. Rev. X* **4**, 011017 (2014).

[12] M. A. Taylor and W. P. Bowen, *Physics Reports* **615**, 1 (2016).

[13] R. Whittaker, C. Erven, A. Neville, M. Berry, J. L. O'Brien, H. Cable, and J. C. F. Matthews, *New Journal of Physics* **19**, 023013 (2017).

[14] R. Cole, *Cell Adhesion & Migration* **8**, 452 (2014).

[15] F. Wolfgramm, C. Vitelli, F. A. Beduini, N. Godbout, and M. W. Mitchell, *Nature Photonics* **7**, 28 (2012).

[16] S. F. Huelga, C. Macchiavello, T. Pellizzari, A. K. Ekert, M. B. Plenio, and J. I. Cirac, *Phys. Rev. Lett.* **79**, 3865 (1997).

[17] Y. Matsuzaki, S. C. Benjamin, and J. Fitzsimons, *Phys. Rev. A* **84**, 012103 (2011).

[18] A. W. Chin, S. F. Huelga, and M. B. Plenio, *Phys. Rev. Lett.* **109**, 233601 (2012).

[19] R. Chaves, J. B. Brask, M. Markiewicz, J. Kołodyński, and A. Acín, *Phys. Rev. Lett.* **111**, 120401 (2013).

[20] J. B. Brask, R. Chaves, and J. Kołodyński, *Phys. Rev. X* **5**, 031010 (2015).

[21] A. Smirne, J. Kołodyński, S. F. Huelga, and R. Demkowicz-Dobrzański, *Phys. Rev. Lett.* **116**, 120801 (2016).

[22] S. Haroche and J.-M. Raimond, *Exploring the Quantum*, Vol. 5 (Oxford University Press, 2006) p. 11.

[23] A. Blais, S. M. Girvin, and W. D. Oliver, *Nature Physics* **16**, 247 (2020).

[24] C. W. Helstrom, *Quantum Detection and Estimation Theory* (Elsevier Science, 1976).

[25] A. S. Holevo, *Probabilistic and Statistical Aspects of Quantum Theory (Statistics & Probability) (English and Russian Edition)* (Elsevier Science, 1982).

[26] S. L. Braunstein and C. M. Caves, *Phys. Rev. Lett.* **72**, 3439 (1994).

[27] R. A. Campos, C. C. Gerry, and A. Benmoussa, *Phys. Rev. A* **68**, 023810 (2003).

[28] M. G. A. Paris, *International Journal of Quantum Information* **07**, 125 (2009).

[29] T. Kim, O. Pfister, M. J. Holland, J. Noh, and J. L. Hall, *Phys. Rev. A* **57**, 4004 (1998).

[30] L. Pezzé and A. Smerzi, *Phys. Rev. Lett.* **110**, 163604 (2013).

[31] S. Knysh, V. N. Smelyanskiy, and G. A. Durkin, *Phys. Rev. A* **83**, 021804 (2011).

[32] B. Escher, R. de Matos Filho, and L. Davidovich, *Nature Physics* **7**, 406 (2011).

[33] R. Demkowicz-Dobrzański, J. Kołodyński, and M. Gută, *Nature Communications* **3** (2012), 10.1038/ncomms2067.

[34] J. Kołodyński and R. Demkowicz-Dobrzański, *New Journal of Physics* **15**, 073043 (2013).

[35] S. D. Huver, C. F. Wildfeuer, and J. P. Dowling, *Phys. Rev. A* **78**, 063828 (2008).

[36] U. Dorner, R. Demkowicz-Dobrzanski, B. J. Smith, J. S. Lundeen, W. Wasilewski, K. Banaszek, and I. A. Walmsley, *Phys. Rev. Lett.* **102**, 040403 (2009).

[37] R. Demkowicz-Dobrzanski, U. Dorner, B. J. Smith, J. S. Lundeen, W. Wasilewski, K. Banaszek, and I. A. Walmsley, *Phys. Rev. A* **80**, 013825 (2009).

[38] H. Cable and G. A. Durkin, *Phys. Rev. Lett.* **105**, 013603 (2010).

[39] J. Calsamiglia, B. Gendra, R. Muñoz-Tapia, and E. Bagan, *New Journal of Physics* **18**, 103049 (2016).

[40] A. González-Tudela, V. Paulisch, H. J. Kimble, and J. I. Cirac, *Phys. Rev. Lett.* **118**, 213601 (2017).

[41] V. Paulisch, M. Perarnau-Llobet, A. González-Tudela, and J. I. Cirac, *Phys. Rev. A* **99**, 043807 (2019).

[42] M. Perarnau-Llobet, A. González-Tudela, and J. I. Cirac, *Quantum Science and Technology* **5**, 025003 (2020).

[43] D. Malz and J. I. Cirac, arXiv preprint arXiv:1906.12296 (2019).

[44] H. Zhang, R. McConnell, S. Ćuk, Q. Lin, M. H. Schleier-Smith, I. D. Leroux, and V. Vuletić, *Physical Review Letters* **109**, 133603 (2012).

[45] D. B. Hume, I. Stroescu, M. Joos, W. Muessel, H. Strobel, and M. K. Oberthaler, *Physical Review Letters* **111**, 253001 (2013), arXiv:1307.7598.

[46] F. Haas, J. Volz, R. Gehr, J. Reichel, and J. Esteve, *Science* **344**, 180 (2014).

[47] E. Jeffrey, D. Sank, J. Y. Mutus, T. C. White, J. Kelly, R. Barends, Y. Chen, Z. Chen, B. Chiaro, A. Dunsworth, A. Megrant, P. J. J. O’Malley, C. Neill, P. Roushan, A. Vainsencher, J. Wenner, A. N. Cleland, and J. M. Martinis, *Physical Review Letters* **112**, 190504 (2014).

[48] T. Walter, P. Kurpiers, S. Gasparinetti, P. Magnard, A. Potočnik, Y. Salathé, M. Pechal, M. Mondal, M. Oppliger, C. Eichler, and A. Wallraff, *Physical Review Applied* **7**, 054020 (2017).

[49] R. Dassonneville, T. Ramos, V. Milchakov, L. Planat, Dumur, F. Foroughi, J. Puertas, S. Leger, K. Bharadwaj, J. Delaforce, C. Naud, W. Hasch-Guichard, J. J. García-Ripoll, N. Roch, and O. Buisson, *Physical Review X* **10**, 11045 (2020).

[50] M. W. Mitchell, *Quantum Science and Technology* **2**, 044005 (2017).

[51] R. J. Thompson, G. Rempe, and H. J. Kimble, *Physical Review Letters* **68**, 1132 (1992).

[52] M. Brune, F. Schmidt-Kaler, A. Maali, J. Dreyer, E. Hagley, J. M. Raimond, and S. Haroche, *Physical Review Letters* **76**, 1800 (1996).

[53] T. Yoshie, A. Scherer, J. Hendrickson, G. Khitrova, H. M. Gibbs, G. Rupper, C. Ell, O. B. Shchekin, and D. G. Deppe, *Nature* **432**, 200 (2004).

[54] A. Wallraff, D. I. Schuster, A. Blais, L. Frunzio, R.-S. Huang, J. Majer, S. Kumar, S. M. Girvin, and R. J. Schoelkopf, *Nature* **431**, 162 (2004).

[55] J. P. Reithmaier, G. Sek, A. Löfller, C. Hofmann, S. Kuhn, S. Reitzenstein, L. V. Keldysh, V. D. Kulakovskii, T. L. Reinecke, and A. Forchel, *Nature* **432**, 197 (2004).

[56] I. Chiorescu, P. Bertet, K. Semba, Y. Nakamura, C. J. P. M. Harmans, and J. E. Mooij, *Nature* **431**, 159 (2004).

Classical Fisher Information for number-resolved measurements

In this section we compute the classical Fisher information,

$$\mathcal{F}_C = \sum_j \frac{1}{q_j} \dot{q}_j^2, \quad (12)$$

where q_j is the probability to obtain outcome j , for number resolved measurements in the set-up described in the main text. Because of the map between our framework and Mach-Zehnder interferometry with symmetric (time-dependent) photon loss, we can follow similar derivations in that context, see e.g. Refs. [29, 30]. Let us first compute the probabilities of the photon-number measurements for the initial Fock state $|k, m\rangle$ and unitary $U_g = e^{-itH_0}e^{-itH_{\text{int}}}$. First of all we note that e^{-itH_0} commutes with the initial state (with a well defined photon number in each arm) and hence can be ignored for the number-resolved statistics. We first compute:

$$P(k, m, q, g) \equiv |\langle k - q, m + q | e^{-igtH_{\text{int}}} |k, m\rangle|^2 \quad (13)$$

with $|k, m\rangle = \frac{1}{\sqrt{k!m!}}(a^\dagger)^k(b^\dagger)^m|0, 0\rangle$ and $q \in [-m, k]$. Noting that:

$$\begin{aligned} a_g^\dagger &\equiv e^{-igtH_{\text{int}}} a^\dagger e^{igtH_{\text{int}}} = a^\dagger \cos\left(\frac{tg}{2}\right) + i b^\dagger \sin\left(\frac{tg}{2}\right) \\ b_g^\dagger &\equiv e^{-igtH_{\text{int}}} b^\dagger e^{igtH_{\text{int}}} = b^\dagger \cos\left(\frac{tg}{2}\right) + i a^\dagger \sin\left(\frac{tg}{2}\right), \end{aligned} \quad (14)$$

we obtain

$$P(k, m, q, g) = \frac{(m+q)!(k-q)!}{m!k!} (\tan \theta)^{2q} \left(\sum_{j=0}^m \binom{m}{j} \binom{k}{j+q} (-1)^j (\cos \theta)^{k+m-2j} (\sin \theta)^{2j} \right)^2 \quad (15)$$

where we defined $\theta \equiv tg/2$, and $q \in [-m, k]$. This can also be expressed as:

$$\begin{aligned} P(k, m, q, g) &= \frac{(m+q)!(k-q)!}{m!k!} (\tan \theta)^{2q} \\ &\quad \left((-1)^k \binom{m}{k+1} \binom{k}{k+q+1} \frac{(\sin \theta)^{2k+2}}{(\cos \theta)^{2m-k}} {}_3F_2(1, -m+k+1, q+1; k+2, k+q+2; -\tan^2(\theta)) \right. \\ &\quad \left. + \binom{k}{q} (\cos \theta)^{m+k} {}_2F_1(-m, q-k; q+1; -\tan^2(\theta)) \right)^2, \end{aligned} \quad (16)$$

where ${}_pF_q(a; b; z)$ is the generalized hypergeometric function.

Next, we compute the probability to obtain outcomes $\{k, m\}$ for the state:

$$\rho = \sum_{k,j} p_k p_j |n-k, n-j\rangle \langle n-k, n-j| \quad (17)$$

with

$$p_k = \mu^k (1-\mu)^{n-k} \binom{n}{k}, \quad \mu = 1 - e^{-\gamma t}. \quad (18)$$

It is convenient to introduce:

$$\begin{aligned} n_{\text{loss}} &\equiv 2n - (k+m) \\ q &\equiv n - k \end{aligned} \quad (19)$$

Then, we have for (17)

$$P^{\text{Fock}}(n_{\text{loss}}, q, g) = \sum_{l=0}^{n_{\text{loss}}} p_l p_{n_{\text{loss}}-l} P(n-l, n+l-n_{\text{loss}}, q-l, g) \quad (20)$$

The only remaining step is to compute the classical Fisher information using (12):

$$\mathcal{F}_C(g) = \sum_{n_{\text{loss}}=0}^{2n} \sum_{q=n_{\text{loss}}-n}^n \frac{(\partial_g P^{\text{Fock}}(n_{\text{loss}}, q, g))^2}{P^{\text{Fock}}(n_{\text{loss}}, q, g)} \quad (21)$$

To gain some analytical insight for this expression, we can compute it in the limit $g \rightarrow 0$. Following [30, 42], we can expand the probabilities around $g \approx 0$ up to order $\mathcal{O}(g^2)$, which leads to the following analytical expression for the CFI:

$$\lim_{g \rightarrow 0} \mathcal{F}_C(g) = 2t^2(n+1)n(1-\mu)^{n+1}, \quad (22)$$

which shows an exponential decay with $n = N/2$. This is hence far from \mathcal{F}_Q for large N , while still better than NOON states.

Finally, we numerically compute (21) for different g , μ and N for the state (17) (and setting $t = 1$). An example is shown in Fig. 4, from it we see that in general the dependence of \mathcal{F}_C with g is non-trivial, and so is the point where it is maximized. The figure also shows that indeed (12) does not saturate \mathcal{F}_Q for number-resolved measurements. In Fig. 4 we also show (21) as a function of N , where it becomes apparent the importance of maximizing \mathcal{F}_C with respect to g for the number-resolved-measurements as N increases. The numerical results suggest that a systematic improvement with respect to the Shot-Noise-Limit can be obtained for any N with suitably optimized number-resolved-measurements.

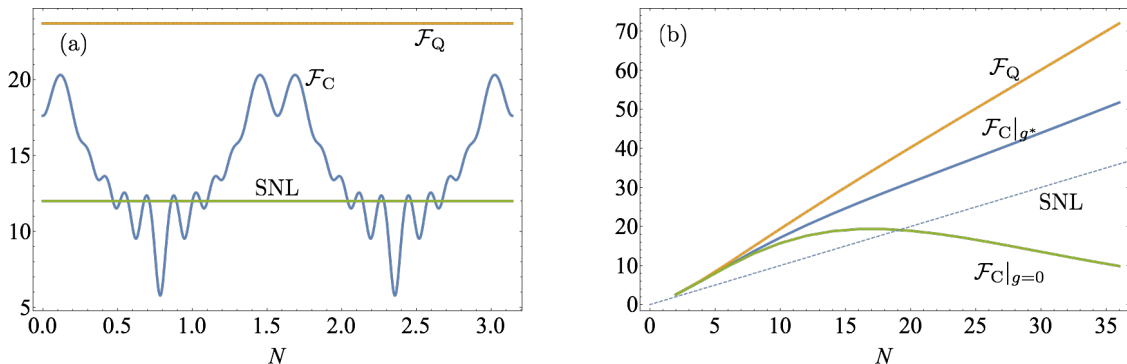


Figure 4. (a) CFI, QFI, and SNL vs ϕ . Parameters: $N = 12$, $\mu = 0.2$, and $t = 1$. (b) \mathcal{F}_Q and \mathcal{F}_C vs N for $\mu = 0.2$ and $t = 1$.

Let us now look at the Poisson limit $N \rightarrow \infty$, $t \rightarrow 0$ while satisfying $2\gamma tn \rightarrow N_{\text{abs}}$. First, from (22), we can study the Poisson limit $2\gamma tn \rightarrow N_{\text{abs}}$, where we obtain:

$$\lim_{g \rightarrow 0} \mathcal{F}_C = \frac{N_{\text{abs}}^2}{2\gamma^2} e^{-N_{\text{abs}}/2}. \quad (23)$$

To obtain similar analytical expression for arbitrary g is challenging due to the complexity of obtaining asymptotic expressions for the generalized hypergeometric functions. Yet, we can obtain numerical results for rather large $N \approx 100 - 1000$. To do this, it is useful to approximate \mathcal{F}_C in (21) as:

$$\mathcal{F}_C(g) \approx \sum_{n_{\text{loss}}=0}^{N_{\text{loss}}^{\max}} \sum_{q=-q_{\max}}^{q_{\max}} \frac{(\partial_g P^{\text{Fock}}(n_{\text{loss}}, q, g))^2}{P^{\text{Fock}}(n_{\text{loss}}, q, g)} \quad (24)$$

since only terms with $q = \mathcal{O}(1)$ and $N_{\text{loss}}^{\max} = \mathcal{O}(N_{\text{abs}})$ contribute to the sum in the Poisson limit (other terms are exponentially small). In our numerical simulations, we take $q_{\max} = 10$ and $N_{\text{loss}}^{\max} = 4N_{\text{abs}}$, and the results become in practice indistinguishable when these parameters are varied. Numerical results are shown in Fig. 2 of the main text.

Optimal measurement

Finally, we note that the optimal measurement L where the classical Fisher info (12) saturates Q is given by [28]:

$$\begin{aligned} L &= i \sum_{k,l} \frac{\tilde{p}_k \tilde{p}_l - \tilde{p}_{k-1} \tilde{p}_{l+1}}{\tilde{p}_k \tilde{p}_l + \tilde{p}_{k-1} \tilde{p}_{l+1}} \sqrt{k(l+1)} \left(|k, l\rangle \langle k-1, l+1| + |l, k\rangle \langle l+1, k-1| \right) \\ &= i \sum_{k,l} \frac{(n-k+1)(l+1) - k(n-l)}{n(l+k+1) + k(n-l)} \sqrt{k(l+1)} \left(|k, l\rangle \langle k-1, l+1| + |l, k\rangle \langle l+1, k-1| \right). \end{aligned} \quad (25)$$

with $\tilde{p}_k = p_{n-k}$. In the presence of photon loss (i.e. $p_0 \neq 1$), this does not correspond to a number resolved measurement of the two modes, but to a global measurement involving both modes.

Implementation in Cavity QED

In this section we discuss the measurement precision (both QFI and CFI) for the proposed implementation. At each run of the experiment, the initial state is a Fock state: $|m, l\rangle$, where the photon number m, l are known. The interaction time $t_{m,l}$ between cavities is taken such that given m, l initial photons, at most N_{abs} photons are absorbed, i.e.:

$$N_{\text{abs}} = (m+l)(1 - e^{-\gamma t_{m,l}}). \quad (26)$$

We then repeat the experiment until the accumulated time $\sum_{m,l} \nu_{m,l} t_{m,l}$ reaches T , where T is the maximal time of the protocol. We assume the total time T and N_{abs} to be limited. We are interested in the regime $\nu \equiv \sum_{m,l} \nu_{m,l} \gg 1$ (i.e. $T/t_{m,l} \gg 1$), where the statistics are dominated by typical sequences in which $\nu_{m,l} = q(m)q(l)\nu$ which, together with $T = \sum_{m,l} \nu_{m,l} t_{m,l}$, provides ν .

Quantum Fisher Information

Assuming a large number of runs of the experiment $\nu \gg 1$ (so that enough statistics for each m, l are obtained), the measurement uncertainty $(\Delta\varphi)^{-2}$ is bounded by

$$(\Delta g)^{-2}_{\text{AC}} \equiv \sum_{m,l} \nu_{m,l} \mathcal{F}_{\text{Q}}^{m,l} = \frac{T}{\sum_{m,l} q(m)q(l)t_{m,l}} \sum_{m,l} q(m)q(l) \mathcal{F}_{\text{Q}}^{m,l} \equiv (\Delta g)^{-2}_{\text{AC}} \quad (27)$$

with $\mathcal{F}_{\text{Q}}^{m,l}$ is the QFI for an initial Fock state $|m, l\rangle$, and it reads (this is a generalisation of Eq. (7) in the main text):

$$\mathcal{F}_{\text{Q}}^{m,l} = 2t_{m,l}^2 \sum_i^l \sum_j^m p_i p_j \left[(l-i)(m-j+1) \left(\frac{1}{2} - \frac{1}{1 + \frac{(m-j+1)(i+1)}{j(l-i)}} \right) + (m-j)(l-i+1) \left(\frac{1}{2} - \frac{1}{1 + \frac{(l-i+1)(j+1)}{i(m-j)}} \right) \right] \quad (28)$$

In Fig. 5 we plot the upper bound (27) compared to twin Fock states with $2n$ photons. We observe that the ratio $(\Delta g)^{-2}_{\text{AC}}/(\Delta g)^{-2}_{\text{TFS}}$ converges to ≈ 0.7 , showing that the proposed implementation performs well.

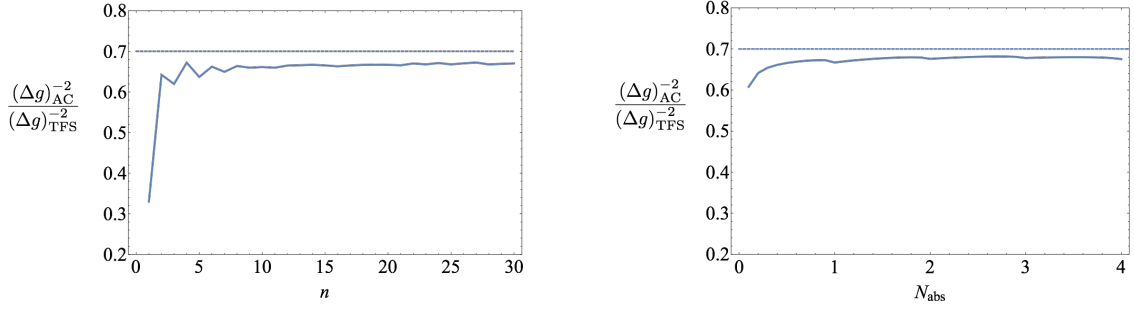


Figure 5. (a) $(\Delta g)_{\text{AC}}^{-2}/(\Delta g)_{\text{TFS}}^{-2}$ vs n . Parameters: $\gamma = 1$, $T = 10$, and $N_{\text{abs}} = 1$. (b) $(\Delta g)_{\text{AC}}^{-2}/(\Delta g)_{\text{TFS}}^{-2}$ vs N_{abs} . Parameters: $\gamma = 1$, $T = 10$, and $n = 20$.

Asymptotics. Let us attempt to evaluate $(\Delta g)_{\text{AC}}^{-2}/(\Delta g)_{\text{TFS}}^{-2}$ in the regime $m, l \gg 1$. Let us define $N = m + l$ and $m = \alpha N$, $l = \beta N$, while noting that $N_{\text{abs}} = N\gamma t_{m,l}$ for $N \gg 1$. Then, in the limit $N \rightarrow \infty$ while keeping N_{abs} constant:

$$\mathcal{F}_{\text{Q}}^{\alpha,\beta} \equiv \lim_{N \rightarrow \infty} \mathcal{F}_{\text{Q}}^{N\alpha,N\beta} = 2 \frac{N_{\text{abs}}^2}{\gamma^2} \frac{\alpha\beta}{(\alpha + \beta)^2} \sum_{i,j}^{\infty} p_i p_j \left(1 - \frac{j}{j + (i+1)\frac{\alpha}{\beta}} - \frac{i}{i + (j+1)\frac{\beta}{\alpha}} \right) \quad (29)$$

To proceed further we need to know $q_{\alpha} \equiv q(\alpha N)$, which we don't. Let us hence make an educated guess (from Fig. 3), namely:

$$\begin{aligned} q_{\alpha} &= \frac{b}{1 - e^{-b}} e^{-b(1-\alpha)} \\ \int_0^1 \alpha q_{\alpha} &= 0.78 \end{aligned} \quad (30)$$

the second condition yielding $b \approx 4.27$. We then compute the ratio:

$$\lim_{N \rightarrow \infty} \frac{(\Delta g)_{\text{AC}}^{-2}}{(\Delta g)_{\text{TFS}}^{-2}} = \frac{1}{2\mathcal{F}_{\text{Q}}^{1,1}} \frac{\int d\alpha d\beta q_{\alpha} q_{\beta} \mathcal{F}_{\text{Q}}^{\alpha,\beta}}{\int d\alpha d\beta \frac{q_{\alpha} q_{\beta}}{\alpha + \beta}} \approx 0.7, \quad (31)$$

which explains qualitatively well the numerical results.

Classical Fisher Information

It is also interesting to investigate \mathcal{F}_{C} for number-resolved measurements. Analogously with our previous considerations, we have,

$$(\Delta g)_{\text{NRM}}^{-2} = \frac{T}{\sum_{m,l} q(m)q(l)t_{m,l}} \sum_{m,l} q(m)q(l)\mathcal{F}_{\text{C}}^{m,l} \quad (32)$$

with

$$\mathcal{F}_{\text{C}}^{m,l} = \sum_{n_{\text{loss}}=0}^{m+l} \sum_{q=n_{\text{loss}}-l}^m \frac{(\partial_g P^{\text{DickeF}}(n_{\text{loss}}, q, g))^2}{P^{\text{DickeF}}(n_{\text{loss}}, q, g)} \quad (33)$$

with

$$P^{\text{DickeF}}(n_{\text{loss}}, q, g) = \sum_{s=0}^{n_{\text{loss}}} p_{s,m} p_{n_{\text{loss}}-s,l} P(m-s, l+s-n_{\text{loss}}, q-s, g) \quad (34)$$

with $P(m-s, l+s-n_{\text{loss}}, q-s, g)$ given in (16) with $t = t_{m,l}$ and with

$$p_{k,n} = \mu^k (1-\mu)^{n-k} \binom{n}{k}, \quad \mu = 1 - e^{-\gamma t_{m,l}}. \quad (35)$$

Some numerical results are shown in Fig. 6 in the regime $g \approx 0$, where we see that Dicke-Fock states perform reasonably similar than Fock states, even improving on them for large N_{abs} (note that Fock states become exponentially bad with N_{abs} around $g = 0$). More results, including results for an optimal g where the CFI is maximised, g^* , are shown in the main text. As expected, the CFI is always smaller than the QFI.

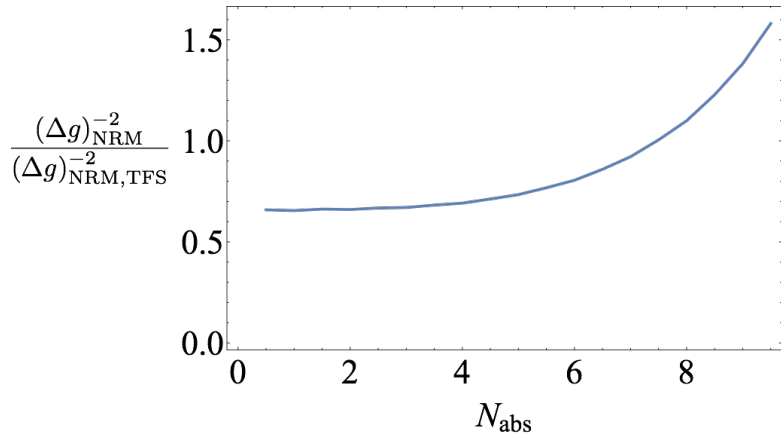


Figure 6. Ratio $\frac{(\Delta g)_{\text{NRM}}^{-2}}{(\Delta g)_{\text{NRM,TFS}}^{-2}}$ vs N_{abs} for $\gamma = 1$, $T = 100$, and at $g \approx 0$. Numerics are done for $n = 20$.

Further experimental consideration

In practice, there are several additional sources of error in this protocol that ought to be considered.

First, we have assumed that all atoms/qubits are exactly on resonance with the cavity. Realistically, they may have differing energies and be detuned from the cavity, which makes the photon exchange between cavity and atoms less efficient. However, measuring the number of excited atoms after the interaction period still projects the cavity state onto a Fock state, such that disorder only affects the probability distribution of the produced Fock states, but not their fidelity.

Second, the fidelity of the generated Fock state is intrinsically limited by measurement error in the atomic readout. High-fidelity atom readout has already been demonstrated for large numbers of atoms in cavity QED [44–46] and for intermediate numbers of qubits in circuit QED [47–49].

Third, the atoms need to be reset to ground state in a time much faster than $1/g$. This is feasible if the cavity coupling is tunable (e.g., via an intermediate resonator in circuit QED) or if a fast decay channel is used (e.g., a fast optical transition of the atom).

Fourth, no photons may be lost throughout the experiment. This requires ultra-high finesse cavities or long qubit coherence times on the scale of $1/g$, i.e., this requires the strong coupling regime, which has been achieved in both cavity and circuit QED [51–56]. While the measurement is more challenging than the preparation, it relies on the same experimental figures of merit. A large advantage of our scheme is that one can post-select on successful runs of the experiment by requiring that at the end $N_a + N_b$ excitations are measured.

Optimal time scale obtained from mean field

Let us consider the Hamiltonian

$$H_2 = \frac{1}{2}a^\dagger b^2 + \text{H.c.}, \quad (36)$$

where a, b are the annihilation operators for two harmonic oscillators. a corresponds to what formerly was a spin, and b is just the same cavity mode as before. In the subspace spanned by the states $|N - m\rangle_a \otimes |2m\rangle_b$, where $\{|m\rangle\}$ are Fock states of an oscillator, the Hamiltonian is a bi-diagonal matrix

$$\mathcal{H} = \begin{pmatrix} 0 & a_0 & 0 & \cdots \\ a_0 & 0 & a_1 & \\ 0 & a_1 & 0 & \ddots \\ \vdots & & \ddots & \ddots \end{pmatrix}, \quad (37)$$

where

$$a_m = \sqrt{(N - m)(m + 1/2)(m + 1)} \approx (m + 1)\sqrt{N - m}. \quad (38)$$

For large $N - m$ these are essentially the same matrix elements as the actual Hamiltonian (11) and one can check numerically that the dynamics is very similar for large enough N . In the classical limit, we replace

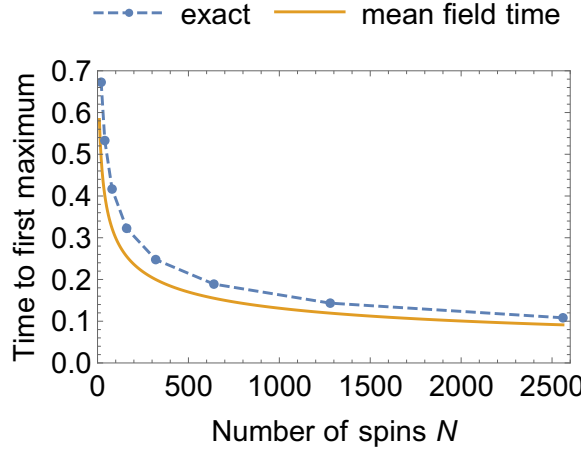


Figure 7. Comparison between the time scale obtained in mean field [Eq. (44)] and the exact timescale calculated numerically.

the annihilation operators by the amplitudes of the corresponding coherent states. The classical (mean field) equations of motion read

$$\frac{d}{dt} \begin{pmatrix} \alpha \\ \beta \end{pmatrix} = -i \begin{pmatrix} \beta^2/2 \\ \beta^* \alpha \end{pmatrix}, \quad (39)$$

with initial conditions $\beta(0) = 1$, $\alpha(0) = \sqrt{N}$.

Now we do a change of variables, taking $\alpha = a \exp(ix)$, $\beta = b \exp(iy)$, such that

$$\dot{a} = -\frac{b^2}{2} \sin \phi, \quad \dot{x} = -\frac{b^2}{2a} \cos \phi, \quad (40a)$$

$$\dot{b} = +ab \sin \phi, \quad \dot{y} = -a \cos \phi, \quad (40b)$$

where $\phi = x - 2y$. Further defining the constant $K = a^2 + b^2/2$, and the variable $r = a^2 - b^2/2$, we obtain the equations of motion

$$\dot{\phi} = -\frac{K + 3r}{\sqrt{2(K + r)}} \cos \phi, \quad (41a)$$

$$\dot{r} = \sqrt{2(K + r)}(K - r) \sin \phi. \quad (41b)$$

This defines a vector field in a two-dimensional plane, whose closed orbits are the possible trajectories of the system. Since the phase ϕ is ill-defined in the initial state, we can choose it to be $\phi = \pi/2$. In this case, the system is governed only by

$$\dot{r} = \sqrt{2(K + r)}(K - r), \quad (42)$$

which is readily integrated to yield

$$\left[\tanh^{-1} \sqrt{\frac{1 + r/K}{2}} \right]_{r(t_i)}^{r(t_f)} = \sqrt{2K}(t_f - t_i). \quad (43)$$

Since initially, $r/K \simeq 1 - 2/N$ and $K \simeq N$ (taking $\alpha = \sqrt{iN}$ and $\beta = 1$), we conclude that the natural timescale for the switch is

$$T \simeq \frac{1}{2\sqrt{N}} \tanh^{-1} \left(1 - \frac{1}{4N} \right) \approx \frac{\log(4N)}{2\sqrt{N}}. \quad (44)$$

This converges to the actual optimal time scale in the limit of large N as we show in Fig. 7.